Magnetization precession by short-wavelength magnon excitations and spin-transfer torque

Shizhu Qiao,[1] Shishen Yan,[2,*] Shishou Kang,[2] Qiang Li,[3] Yufeng Qin,[4] Yinrui Zhao,[2] Zhiyu Zhang,[1] and Shuqing Li[1]

[1]*Department of Science, Taiyuan Institute of Technology, Taiyuan 030008, China*

[2]*School of Physics, State Key Laboratory of Crystal Materials, Shandong University, Jinan 250100, China*

[3]*College of Physics, Qingdao University, Qingdao 266071, China*

[4]*Department of Applied Physics, School of Information Science and Engineering, Shandong Agricultural University, Taian 271018, China*

(Received 4 September 2017; revised manuscript received 19 November 2017; published 22 January 2018)

The Bloch-Bloembergen equation is extended to study the magnetization precession in a spin-valve structure by taking into account the short-wavelength magnon excitation and spin-transfer torque. A stable magnetization precession is achieved when the transverse relaxation time T_2 is longer than the longitudinal relaxation time T_1. A wide current-density window of stable magnetization precession is found for large T_2 and it broadens with increasing T_2 for fixed T_1. Our simulation results also reveal that short-wavelength magnon excitation can reduce the amplitude of the magnetization precession, which is different from the prediction of the macro-spin Landau-Lifshitz-Gilbert-Slonczewski equation.

DOI: 10.1103/PhysRevB.97.024424

I. INTRODUCTION

Since the pioneering works of Berger and Slonczewski [1,2], spin-transfer torque (STT) has been the subject of much attention, owing to its high applicability in spintronic devices. This effect has been realized in many structures with diverse magnetization textures, such as domain walls, vortices, and skyrmions [3–6].

When it comes to theoretical studies of the STT, generally, the Slonczewski torque $\boldsymbol{\tau}_{\mathrm{STT}}$ is added to the Landau-Lifshitz-Gilbert (LLG) equation, leading to the Landau-Lifshitz-Gilbert-Slonczewski (LLGS) equation [7–11]:

$$\frac{\mathrm{d}\boldsymbol{M}}{\mathrm{d}t} = \gamma\mu_0\boldsymbol{M}\times\boldsymbol{H}_{\mathrm{eff}} + \frac{\alpha}{M_{\mathrm{S}}}\boldsymbol{M}\times\frac{\mathrm{d}\boldsymbol{M}}{\mathrm{d}t} + \boldsymbol{\tau}_{\mathrm{STT}}. \quad (1)$$

Here, $\boldsymbol{M}$, γ, μ_0, α, and M_{S} are the magnetization vector, gyromagnetic ratio, permeability of free space, Gilbert damping factor, and saturation magnetization, respectively. The effective field $\boldsymbol{H}_{\mathrm{eff}}$ includes both external and internal magnetic fields, and the Slonczewski torque $\boldsymbol{\tau}_{\mathrm{STT}}$ is perpendicular to $\boldsymbol{M}$. The form of Eq. (1) makes it clear that in such a macrospin approach to the STT magnetization dynamics, the magnitude of $\boldsymbol{M}$ is assumed to stay unchanged, and the excitation of short-wavelength magnons is neglected [12,13]. This approach is valid in sufficiently small devices comparing with the dimension of domain-wall thickness, because the excitation of magnons with wave vector $k \neq 0$ would then cost an excessive amount of exchange energy in such a small dimension [14].

However, the macrospin LLGS model is limited when nonlinear magnon scatterings are considered. Nonlinear magnon scatterings, generating short-wavelength magnons and redistributing momentum and energy in a magnetic system, play an important role in magnetic relaxation [15,16]. Common low-order nonlinear magnon scatterings include extrinsic two-magnon scattering and intrinsic three- and four-magnon scattering. In the process of two-magnon scattering, one $k = 0$ magnon is annihilated while a degenerate $k \neq 0$ magnon is created. Because the momentum is not conserved in this extrinsic process, defects are required [17–22]. In the ferromagnetic resonance (FMR) experiment of Fe/V multilayer samples [18], resonance linewidth is not a linear function of measuring frequency when an applied magnetic field is parallel to the film plane. This result cannot be explained by Gilbert damping only, and the two-magnon scattering should be included.

In the three-magnon scattering process, one $k = 0$ magnon is annihilated while two magnons with opposite wave vector ($\boldsymbol{k}$ and $-\boldsymbol{k}$) are created to conserve momentum, and $\omega_0 = 2\omega_k$ is required to conserve energy [23–25]. This requirement of spin-wave dispersion relation cannot be fulfilled in ultrathin films, and consequently three-magnon scattering is prohibited [26]. In the four-magnon scattering process, two $k = 0$ magnons are annihilated, while two degenerate magnons with opposite wave vector are created, where both momentum and energy are conserved [26–28]. For the sake of simplicity, one four-magnon scattering could be regarded as two conjugate two-magnon scatterings ($0\rightarrow\boldsymbol{k}$ and $0\rightarrow-\boldsymbol{k}$) happening together mathematically; hereafter, in this paper two-magnon scattering and four-magnon scattering are no longer distinguished from each other unless necessary, although they are physically different.

Short-wavelength magnon excitation is also inevitable in the field of magnonics [29–31], which is a subfield of spintronics concerning structures, devices, and circuits that use spin currents carried by all kinds of magnons of both long and short wavelengths. In this field, STT-based magnon injection is an important technique, because it couples spin waves with a spin-polarized direct electric current directly, and therefore connects magnonics with conventional spintronics [32,33].

One way to deal with this dilemma is micromagnetic simulation [34]. In this method, a magnet is subdivided into many sufficiently small cells, which are about several to tens of

*Corresponding author: shishenyan@sdu.edu.cn

nanometers. Within one such small cell, the excitation of $k \neq 0$ magnons is prohibited for it would cost too much exchange energy, and therefore the LLGS equation is applicable in one cell. Many coupled LLGS equations are deployed to characterize magnetizations of these small cells, and $k \neq 0$ magnons would be excited to minimize the total free energy in a much larger dimension comparing with cell size. Consequently, this leads to drawbacks of surging of computational complexity. What is more, nonlinear magnon scatterings are rather obscure in this method, because there is only one parameter Gilbert damping factor α to describe the relaxation of $k = 0$ magnons in the LLGS equation. Thus, a more distinct and convenient theoretical process is in high demand, which is capable of describing short-wavelength magnon excitation and spin-transfer torque.

Besides the LLG equation, other equations are also brought up to study magnetic relaxation [35], among which the Bloch-Bloembergen (BB) equation is widely applied in magnetic dynamics studies [36–39]. The BB equation was introduced by Bloch in order to study nuclear magnetic relaxation, and was subsequently adopted by Bloembergen to study ferromagnetic relaxation in nickel and supermalloys [40]. It can be written as

$$\frac{\mathrm{d}\boldsymbol{M}}{\mathrm{d}t} = \gamma\mu_0 \boldsymbol{M} \times \boldsymbol{H}_{\mathrm{eff}} - \frac{M_x}{T_2}\mathbf{e}_x - \frac{M_y}{T_2}\mathbf{e}_y - \frac{M_z - M_{\mathrm{S}}}{T_1}\mathbf{e}_z, \tag{2}$$

where T_1 is the longitudinal relaxation time, T_2 is the transverse relaxation time, and $\mathbf{e}_i$ (with $i = x, y, z$) are the Cartesian unit vectors. Measuring susceptibility by FMR, Bloembergen gave T_1 and T_2 of about 0.5 ns at room temperature for supermalloy [40]. Klein *et al.* measured T_1 and T_2 of a single-crystal disk of yttrium-iron garnet (YIG) by magnetic-resonance force microscopy, giving $T_1 = 106$ ns and $T_2 = 162$ ns [41]. Considering the ultralow Gilbert damping factor $\alpha \sim 10^{-5}$ of YIG [32], this high value of relaxation time is reasonable comparing with $\alpha \sim 10^{-3}$ of permalloy [42].

In comparison with the LLG equation, the BB equation provides the magnetization vector $\boldsymbol{M}$ with greater freedom. First, the magnitude of $\boldsymbol{M}$ need not be fixed, which means that excitation of short-wavelength magnons can be naturally included in Eq. (2). Second, the transverse components (M_x, M_y) and longitudinal component (M_z) of the magnetization can relax separately, in stark contrast to the relaxation behavior described by the LLG equation.

Using Heisenberg Hamiltonian simulation in the atomic scale, Hellsvik *et al.* found that spin-wave instability occurs when there is a magnetic anisotropy in system at finite temperature. Spin-wave instability leads to a Bloch-Bloembergen-type relaxation of the magnetization, where the magnitude of magnetization changes [38]. Spin-wave instability is also reported in $Ni_{83}Fe_{17}$ thin film, where nonlinear effects become important as soon as the magnetization precession angle exceeds a couple of degrees [43]. The Bloch-Bloembergen equation is also employed in newly developed spintronics. By two alternative approaches, Rezende *et al.* [44] found that both transverse relaxation and longitudinal relaxation used in the Bloch-Bloembergen equation are essential to characterize the spin-pumping damping in thick ferromagnetic films in contact with a nonmagnetic metal layer, such as YIG/Pt.

However, up to now, the BB equation has not been employed to study the magnetic dynamics under spin-transfer torque. Therefore, we add the Slonczewski torque $\boldsymbol{\tau}_{\mathrm{STT}}$ to the BB equation, leading to what may be called the Bloch-Bloembergen-Slonczewski (BBS) equation:

$$\frac{\mathrm{d}\boldsymbol{M}}{\mathrm{d}t} = \gamma\mu_0 \boldsymbol{M} \times \boldsymbol{H}_{\mathrm{eff}} - \frac{M_x}{T_2}\mathbf{e}_x - \frac{M_y}{T_2}\mathbf{e}_y - \frac{M_z - M_{\mathrm{S}}}{T_1}\mathbf{e}_z + \boldsymbol{\tau}_{\mathrm{STT}}. \tag{3}$$

In the following, we can see that a macrospin model based on the BBS equation can be used to study the magnetic dynamics under both short-wavelength magnon excitation and spin-transfer torque. In this paper, a stable magnetization precession can be achieved, and a wide current-density window of stable magnetization precession is found for large T_2, which is favorable for a current-tuning spin-transfer torque oscillator.

II. THEORETICAL MODEL

Here we apply the BBS equation in the form of Eq. (3) to a simple trilayer spin-valve structure sketched in Fig. 1(a), where a thin free magnetic layer and a thick fixed magnetic layer are separated by a nonmagnetic metal layer. Without loss of generality, the uniaxial anisotropy of the thin free magnetic layer is along the z axis, the magnetization of the thick fixed magnetic layer is pinned along the negative z direction, and the applied magnetic field $\boldsymbol{H}_0$ is along the positive z direction. In this case, when the magnetization vector of the free magnetic layer $\boldsymbol{M}$ is pulled from its equilibrium along

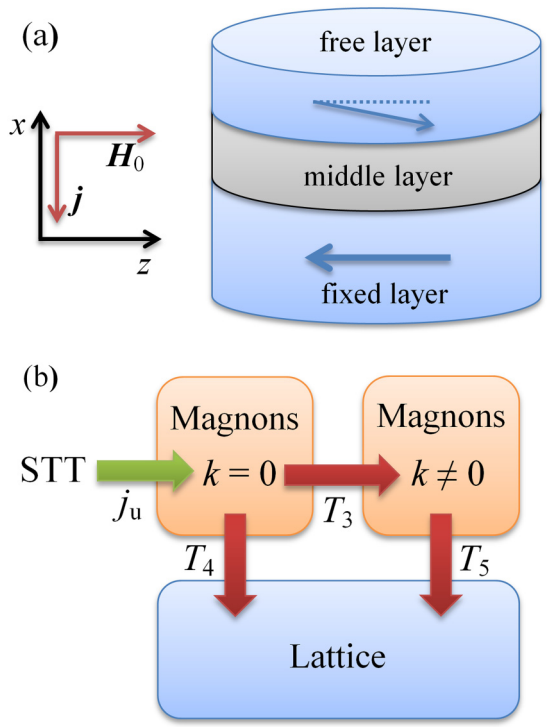

FIG. 1. (a) A trilayer spin-valve structure used in our magnetic dynamics study. (b) Three approaches of magnetization relaxation of the free magnetic layer.

the z axis, the effective field $\boldsymbol{H}_{\rm eff}$ in Eq. (3) acting upon the free magnetic layer includes three components: the applied magnetic field, the uniaxial anisotropy field along the z axis, and the demagnetizing field along the x axis.

When electrons flow from the fixed magnetic layer to the free magnetic layer, the Slonczewski torque $\boldsymbol{\tau}_{\rm STT}$ in Eq. (3) exerting on the free magnetic layer is $\mu_{\rm B} j P \boldsymbol{m} \times (\boldsymbol{m} \times \boldsymbol{f})/de$, where $\mu_{\rm B}$, j, P, $\boldsymbol{m}$, $\boldsymbol{f}$, d, and e are the Bohr magneton, current density, spin polarization, unit vector of the magnetization of the free magnetic layer, unit vector of the magnetization of the fixed magnetic layer, free magnetic layer thickness, and electronic charge, respectively. Therefore, the Slonczewski torque $\boldsymbol{\tau}_{\rm STT}$ only changes the direction of $\boldsymbol{M}$ rather than the magnitude. In other words, it only injects $k = 0$ magnons into the free magnetic layer.

Now we turn to discuss the possible mechanisms of magnetization relaxation of the free magnetic layer in the trilayer spin-valve structure, which may reveal the detailed origins of T_1 and T_2 in Eq. (3). Following Suhl's work [14], as shown in Fig. 1(b), the magnetization relaxes through three approaches [16,45–47].

First, magnons with $k = 0$ are scattered, and subsequently turn into magnons with $k \neq 0$. This process is known as two-magnon scattering, and is characterized by the relaxation time T_3, which is inversely proportional to the square of the matrix element of this scattering Hamiltonian [35]. This relaxation process could be significant or even dominant when the magnetization precession angle is sufficiently larger. Through micromagnetic simulation, Dobin and Victora gave the relaxation time of this magnon scattering process shorter than 1.2 ns when the rotation angle is larger than 20° [26]. In the FMR experiment of 1.0-nm epitaxial Fe on GaAs substrate, two-magnon scattering has in-plane anisotropy, and the scattering strength is ranging from 0.2 to 5.2 GHz depending on azimuthal angle [21]. FMR measurement of Fe/V multilayers gives similar results [18].

As the definition of magnon, the excitation of one magnon reduces M_z by $g\mu_{\rm B}$, where g is the g factor [16]. Consequently, in the first approach, the longitudinal component of magnetization (M_z) stays unchanged, because the number of all magnons is unchanged. The excitation of $k \neq 0$ magnons reduces the magnitude of magnetization, because magnetization at each cell does not precess coherently due to $k \neq 0$ magnons [16]. Therefore, the magnitude of magnetization $\boldsymbol{M}$ decreases for the number of $k \neq 0$ magnons is increased in this magnon scattering process, and as a result, the transverse components (M_x, M_y) decrease. This means that the relaxation time T_3 contributes to T_2, but it does not contribute to T_1.

Second, the magnons with $k = 0$ are coupled to the lattice system by a spin-lattice relaxation process characterized by relaxation time T_4, which is about a few nanoseconds [48]. Spin-lattice relaxation could be caused by magnon-electron scattering, magnon-phonon scattering, and Kambersky-Korenman-Prange spin-orbit mediated scattering [26,49,50]. In the second approach, the longitudinal component (M_z) increases, because the number of all magnons is decreased in this process. The number of $k \neq 0$ magnons is not affected and the magnitude of magnetization $\boldsymbol{M}$ stays unchanged, leading to the decrease of transverse components (M_x, M_y). This means that the relaxation time T_4 contributes to both T_1 and T_2.

TABLE I. Default values of parameters used in our simulations. $M_{\rm S}, H_{\rm K}, d, P, j, T_3$, and T_4 are the saturation magnetization, uniaxial anisotropy field, thickness of the free magnetic layer, spin polarization, current density passing through device, two-magnon scattering relaxation time, and spin-lattice relaxation time of $k = 0$ magnons, respectively.

Parameter	Value	Parameter	Value
$M_{\rm S}$	8×10^5 A/m	j	2.3×10^{11} A/m^2
$H_{\rm K}$	2.9×10^4 A/m	T_3	1 ns
d	2.5 nm	T_4	1 ns
P	0.3	T_5^*	1 ns

Third, the magnons with $k \neq 0$ are also coupled to the lattice system by a spin-lattice relaxation process, and its relaxation time T_5 is on the order of 1 ns [26]. Because the total magnons and the $k \neq 0$ magnons are both decreasing in the third approach, the longitudinal component (M_z) increases and the magnitude of magnetization $\boldsymbol{M}$ also increases. However, the magnons with $k \neq 0$ do not affect the transverse components (M_x, M_y) [45]. This means that the relaxation time T_5 only contributes to T_1.

Considering the above three approaches, we have $1/T_2 = 1/T_3 + 1/T_4$ [16,45] in Eq. (3). On the other hand, we can write the differential equation of relaxation of $k = 0$ magnons as $\mathrm{d}n_{\rm u}/\mathrm{d}t = j_{\rm u}/d - n_{\rm u}/T_2$, where $n_{\rm u}$ is the density of $k = 0$ magnons, and $j_{\rm u}$ is the injecting $k = 0$ magnon current density due to STT. For the $k \neq 0$ magnons, we have $\mathrm{d}n_{\rm d}/\mathrm{d}t = n_{\rm u}/T_3 - n_{\rm d}/T_5$, where $n_{\rm d}$ is the density of $k \neq 0$ magnons. Adding these two differential equations together, we have $1/T_1 = 1/T_4 + 1/T_5^*$ and $1/T_5^* = (1/T_5 - 1/T_4)n_{\rm d}/(n_{\rm u} + n_{\rm d})$ [45,51] in Eq. (3).

It is clear that the above three approaches are well included in the macro-spin BBS model. However, the magnitude of magnetization $\boldsymbol{M}$ always stays unchanged in the macrospin LLGS model in the form of Eq. (1), so the first and the third approaches cannot be described by the macrospin LLGS model in spite of the second approach [35]. This further highlights the main difference between the BBS equation and the LLGS equation.

III. CALCULATION RESULTS AND DISCUSSION

The following simulations and discussions are based on Eq. (3) and Fig. 1. Unless otherwise specified, the values of the various parameters used in our simulations are listed in Table I [8,40], where we assign 1 ns to T_5^* in order to fix the T_1 value. $M_{\rm S}, H_{\rm K}$, and P in Table I are based on the parameters of $Ni_{80}Fe_{20}$ alloy.

In order to demonstrate the impacts of the two-magnon scattering process (i.e., the excitation of short-wavelength magnons) on magnetic precession under STT, we simulate Eq. (3) with different relaxation time $T_3 = 0.6$, 0.8, 1, and 1.2 ns, respectively, and the results of our simulations are shown in Fig. 2. For the $T_3 = 0.6$ ns case with relatively strong two-magnon scattering, the amplitude of M_x (and that of M_y) attenuates toward zero, as shown in Fig. 2(a). Meanwhile, both M_z and M (the magnitude of magnetization $\boldsymbol{M}$) relax toward $M_{\rm S}$, as shown in Figs. 2(b) and 2(c). These variations

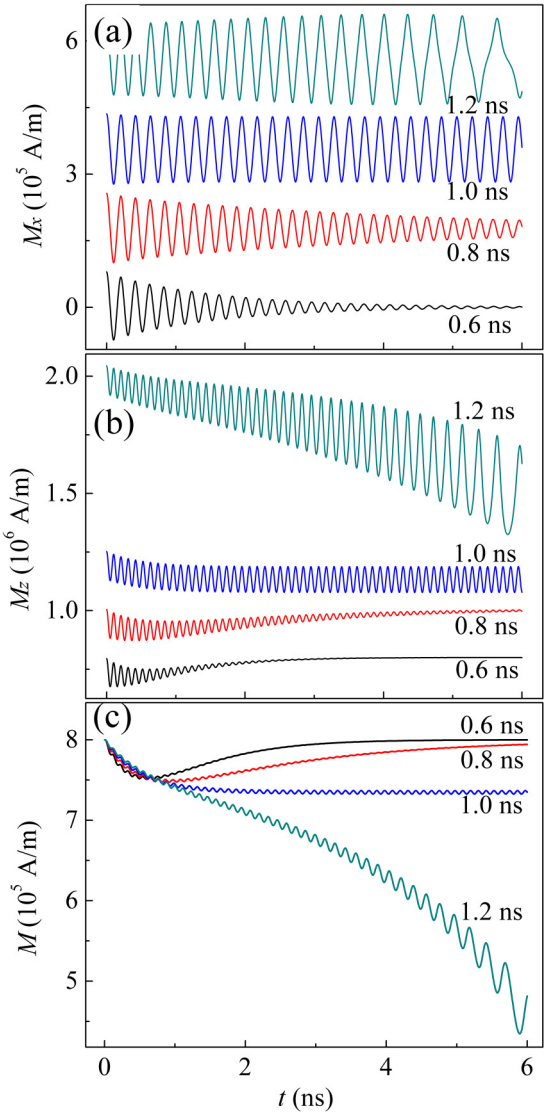

FIG. 2. Magnetization dynamics of the free magnetic layer at different values of T_3: (a) M_x, (b) M_z, and (c) $M = |\boldsymbol{M}|$. In (a) and (b), lines at different T_3 are stacked by vertical axis offset for clearness.

indicate that the magnetization of the free magnetic layer tends to relax to its equilibrium along the z axis. The $T_3 = 0.8$ ns case behaves similarly to the $T_3 = 0.6$ ns one, but in a more moderate way. However, in the $T_3 = 1$ ns case with relatively weak two-magnon scattering, M_x, M_z, and M all oscillate steadily with invariant frequency and amplitude after no more than 2 ns, and this case represents stable magnetization precession. In the $T_3 = 1.2$ ns case, the amplitudes of M_x, M_z, and M all increase, while the envelopes of M_z and M quickly decrease. This case represents magnetization switching. It is worth noting that M varies significantly for all cases, as shown in Fig. 2(c), which is different from macrospin LLGS model prediction.

In Fig. 3(a) we show the stable magnetization precession when $T_3 = 2$ ns ($T_1 = 0.5$ ns and $T_2 = 0.67$ ns) at various current densities from 1.81×10^{11} A/m^2 to 2.1×10^{11} A/m^2. We can see that the envelopes of magnetization quickly decrease in the initial stage and the magnetization gets to a stable precession state very soon for the given current density. Moreover, the stable magnetization precession is obtained with a wide window of the current density, and the amplitude of magnetization increases with the current density.

Figure 3(b) shows the dependence of $j_{\max}$ and $j_{\min}$ on T_2 with fixed T_1 ($T_1 = 0.5$ ns), where $j_{\max}$ and $j_{\min}$ are, respectively, the maximum and minimum current densities for stable precession. Although both $j_{\max}$ and $j_{\min}$ decrease with T_2, the current-density window ($j_{\max} - j_{\min}$) increases with T_2. A wide current-density window is desirable for the STT oscillator community because oscillation frequency can be easily tuned by the current. The inset of Fig. 3(b) further indicates that the oscillation frequency decreases monotonically with the current density, which is similar to the LLGS case [8]. Similar experimental results are reported in the $Co_{90}Fe_{10}/Cu/Ni_{80}Fe_{20}$ point-contact structure [52] and $Ni_{80}Fe_{20}/Cu/Ni_{80}Fe_{20}$ nanopillar structure [53,54], where the latter show frequency jumping at some low current points. Rather different experimental results are also reported in Fe/Ag/Fe pillar structure [55], where uniform precession state and vortex precession state are found under high and low applied field, respectively. The former's frequency dependence on current is weaker than the latter's, and is nonmonotonic, while in the latter scenario, the frequency is monotonic and increasing with current. These experimental results indicate that our macrospin model based on the BBS equation has limitations.

Figure 3(c) shows minimum and maximum stable precession frequency ($f_{\min}$ and $f_{\max}$) corresponding to $j_{\max}$ and $j_{\min}$ in Fig. 3(b). Surprisingly, an increase in T_2 shows little influence on $f_{\max}$, although it changes $j_{\min}$ obviously. On the contrary, $f_{\min}$ increases evidently with the increasing of T_2. In other words, the stable precession frequency window ($f_{\max} - f_{\min}$) shrinks with increasing T_2, although the current-density window broadens dramatically.

The inset of Fig. 3(c) shows the stability of the magnetization precession when $T_3 = 2$ ns for different initial magnetization vectors. Here we set the initial magnetization vectors $M_y(0) = 0$, $M_z(0) = \sqrt{M_S^2 - M_x^2(0)}$, and $M_x(0) = 20, 40, 60$, and 80 kA/m, respectively. It is clear that stable precessions with the same frequency and amplitude are achieved after no more than 15 ns in all cases.

Under the condition of $T_1 > T_2$ (such as $T_3 = 0.8$ ns, i.e., $T_1 = 0.5$ ns, and $T_2 = 0.44$ ns), unstable precession is shown in Fig. 3(d). As shown in Fig. 3(d), the amplitude of M_x attenuates when the current density $j = 2.5395 \times 10^{11}$ A/m^2 (red curve), whereas it increases when the current density $j = 2.5409 \times 10^{11}$ A/m^2 (blue curve), despite the subtle change in current density no more than 0.06%. This means that a stable precession state cannot be achieved even with precise control of the current density for the case of $T_3 = 0.8$ ns, in stark contrast to the $T_3 = 2$ ns case.

Figure 4(a) shows the magnetization trajectories of stable precession of the free magnetic layer in such STT oscillator for different current densities when $T_3 = 2$ ns. We can see that the magnetization vector trajectories are not confined to a spherical surface, which are different from spherical trajectories predicted by the macrospin LLGS model. On the other hand, the opening angle of the magnetization precession

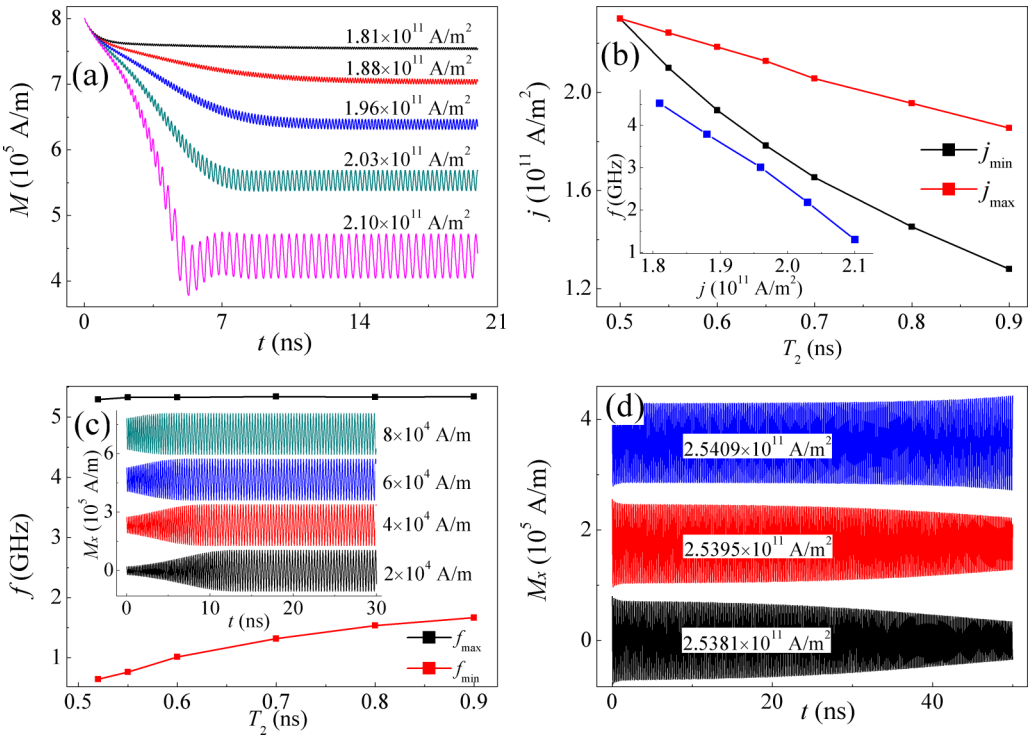

FIG. 3. (a) Stable magnetization precession represented by the evolution of $M = |\boldsymbol{M}|$ for different current densities when $T_3 = 2$ ns (i.e., $T_1 = 0.5$ ns and $T_2 = 0.67$ ns). (b) Minimum and maximum current densities ($j_{\min}$ and $j_{\max}$) for stable magnetization precession at various T_2 with fixed $T_1 = 0.5$ ns; the inset shows the dependence of stable precession frequency on the current density when $T_3 = 2$ ns. (c) Minimum and maximum stable precession frequency ($f_{\min}$ and $f_{\max}$) corresponding to $j_{\max}$ and $j_{\min}$ in (b); the inset of (c) shows the stability of the precession when $T_3 = 2$ ns for different initial magnetization vectors $M_x(0) = 20$, 40, 60, and 80 kA/m, respectively. Lines are stacked by vertical axis offset for clearness. (d) Instability of the precession when $T_3 = 0.8$ ns (i.e., $T_1 = 0.5$ ns and $T_2 = 0.44$ ns) for different current densities. Lines are stacked by vertical axis offset for clearness.

(defined as the maximum angle between the magnetization vector and the z axis during the stable precession) increases with the current density, as shown in Fig. 4(b), which is similar to the prediction of the LLGS simulation [8]. The opening angle is far larger than 20°, which means that the nonlinear magnon-scattering effect is significant, and cannot be neglected [26]. In contrast, the oscillation amplitude of M_y first increases with the current density when the current density is small, but then decreases when the current density is large, as shown in Fig. 4(b), which is different from the LLGS prediction [8]. This behavior is caused by two competing factors: the increasing of the opening angle in Fig. 4(b) and the decreasing of the magnetization magnitude in Fig. 3(a) with the current density.

Besides the STT oscillator, STT magnetic random access memory (STT-MRAM) is another important application of STT, due to its nonvolatile, energy-saving, and short access time features [56]. An interesting point to note is that our simulations and analyses elucidate the different features required in the fabrication of these two kinds of devices. A STT-MRAM device needs to operate in the switching region, so $T_2 < T_1$ is preferable. In contrast, $T_2 > T_1$ should be ensured in the fabrication of the STT oscillator, for it operates in the stable precession region.

Since $1/T_1 = 1/T_4 + 1/T_5^*$ and $1/T_2 = 1/T_3 + 1/T_4$, the relation $T_2 > T_1$ means that the relation $T_3 > T_5^*$ should be fulfilled to obtain stable precession of the STT oscillator. As mentioned before, the relaxation time T_3 describes two-magnon scattering from magnons with $k = 0$ into magnons with $k \neq 0$, so it seems that large T_3 (weak two-magnon scattering) is preferable to achieve stable magnetization precession, which can be tuned by a suitable seed layer [57]. Speaking of the extrinsic two-magnon scattering, fluctuations in the magnetic anisotropy field, small pores, or surface defects can act as scattering centers [19]. In fact, these kinds of scattering centers are common, since STT devices typically feature thin films, fabricated with sophisticated microscale or nanoscale technologies, such as magnetron sputtering, electron beam lithography, and ion etching. Additionally, as an intrinsic process, four-magnon scattering exists even if two-magnon scattering is prohibited for the lack of defects.

However, according to $1/T_5^* = (1/T_5 - 1/T_4)n_d/(n_u + n_d)$, increasing T_3 also leads to the increase of T_5^*. Consequently, the effect of magnon scatterings on the stability of magnetization precession needs further study. Unfortunately, further processing goes beyond this macrospin BBS method, and may need the help of micromagnetic simulation. Short-wavelength magnon excitation related unstable magnetization precession is reported in micromagnetic simulation studies. In nanopillar structures with CoFe or $Ni_{80}Fe_{20}$ as the free magnetic layer, chaotic behaviors in the free magnetic layer are found when a large number of spin-wave modes are generated by excessive spin current, which leads to the breakdown of stable magnetization precession [58,59]. This behavior is markedly different

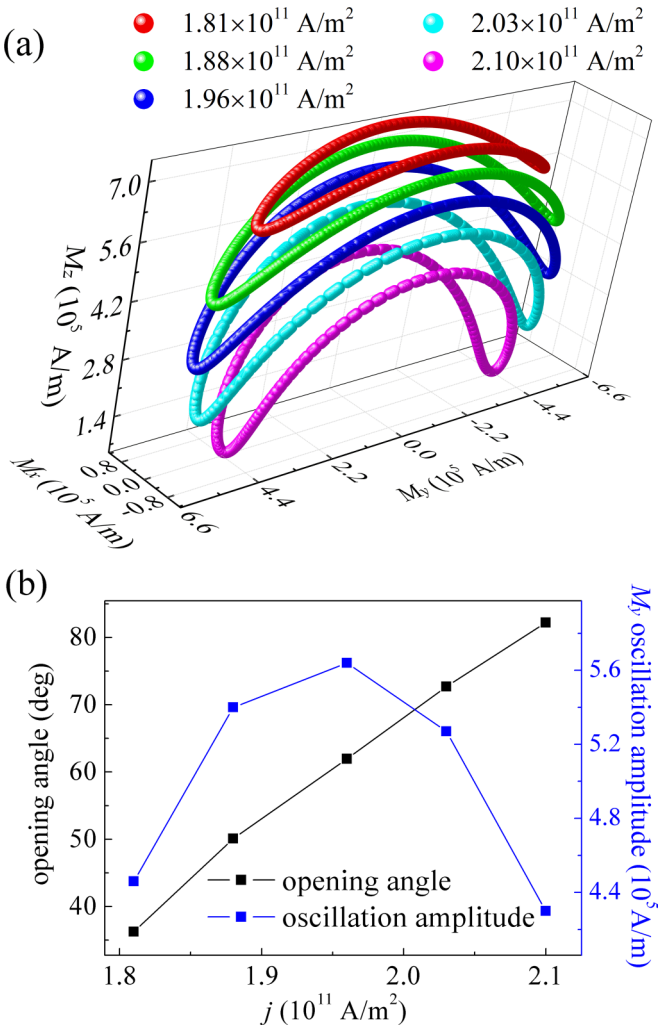

FIG. 4. (a) Stable oscillating magnetization trajectories, and (b) oscillation opening angle and amplitude of M_y for different current densities.

from that predicted by the macrospin LLGS equation. This magnon-scattering issue could be circumvented by shrinking the size of the device to well below the domain-wall thickness of the free magnetic layer, which unfortunately may cut down the output power of the STT oscillator [60]. Under such dimensional restriction, the resulting value of T_3 is then very large and suppresses the excitation of the energetically inefficient $k \neq 0$ magnons [14]. Then the LLGS equation is applicable, and stable magnetization precession is achievable.

IV. CONCLUSIONS

In summary, the Bloch-Bloembergen-Slonczewski equation is established to study the magnetization dynamics of free magnetic layer in a spin-valve structure by taking account of the short-wavelength magnon excitation and spin-transfer torque. The magnetic relaxation process in the free magnetic layer is generalized into three approaches by considering both $k = 0$ and $k \neq 0$ magnons. A stable magnetization precession with wide current-density window can be obtained by achieving $T_2 > T_1$, which is favorable for current-tuning spin-transfer torque oscillator. Our simulation results also reveal that the short-wavelength magnon excitation can reduce the amplitude of the magnetization precession, which is different from the prediction of the macro-spin Landau-Lifshitz-Gilbert-Slonczewski model.

ACKNOWLEDGMENTS

This work is supported by National Natural Science Foundation of China under Grants No. 11647034 and No. 11434006, National Basic Research Program of China under Grant No. 2015CB921502, Program of Shandong Province Higher Educational Science and Technology under Grant No. J17KA184, Program for the Innovative Talents of Taiyuan Institute of Technology under Grant No. 20161011, and Program for the Discipline Leaders of Taiyuan Institute of Technology under Grant No. 20151124.

[1] L. Berger, Phys. Rev. B **54**, 9353 (1996).
[2] J. C. Slonczewski, J. Magn. Magn. Mater. **159**, L1 (1996).
[3] M. Tsoi, A. G. M. Jansen, J. Bass, W.-C. Chiang, M. Seck, V. Tsoi, and P. Wyder, Phys. Rev. Lett. **80**, 4281 (1998).
[4] V. S. Pribiag, I. N. Krivorotov, G. D. Fuchs, P. M. Braganca, O. Ozatay, J. C. Sankey, D. C. Ralph, and R. A. Buhrman, Nat. Phys. **3**, 498 (2007).
[5] S. S. P. Parkin, M. Hayashi, and L. Thomas, Science **320**, 190 (2008).
[6] F. Jonietz, S. Mühlbauer, C. Pfleiderer, A. Neubauer, W. Münzer, A. Bauer, T. Adams, R. Georgii, P. Böni, R. A. Duine, K. Everschor, M. Garst, and A. Rosch, Science **330**, 1648 (2010).
[7] Z. Li and S. Zhang, Phys. Rev. B **68**, 024404 (2003).
[8] M. D. Stiles and J. Miltat, in *Spin Dynamics in Confined Magnetic Structures III*, edited by B. Hillebrands and A. Thiaville (Springer, Berlin, 2006).
[9] D. C. Ralph and M. D. Stiles, J. Magn. Magn. Mater. **320**, 1190 (2008).
[10] B. Lacoste, L. D. Buda-Prejbeanu, U. Ebels, and B. Dieny, Phys. Rev. B **88**, 054425 (2013).
[11] D. J. Byrne, W. T. Coffey, W. J. Dowling, Y. P. Kalmykov, and S. V. Titov, Phys. Rev. B **93**, 064413 (2016).
[12] H. Suhl, *Relaxation Processes in Micromagnetics* (Oxford University Press, New York, 2007).
[13] S. Zhang and S. Zhang, in *Introduction to Spintronics*, edited by C. Bai (Science Press, Beijing, 2014).
[14] H. Suhl, IEEE Trans. Magn. **34**, 1834 (1998).
[15] A. Prabhakar and D. D. Stancil, *Spin Waves Theory and Applications* (Springer, New York, 2009).
[16] M. Sparks, *Ferromagnetic-relaxation Theory* (McGraw-Hill, New York, 1964).
[17] R. Arias and D. L. Mills, Phys. Rev. B **60**, 7395 (1999).
[18] K. Lenz, H. Wende, W. Kuch, K. Baberschke, K. Nagy, and A. Jánossy, Phys. Rev. B **73**, 144424 (2006).
[19] S. S. Kalarickal, P. Krivosik, J. Das, K. S. Kim, and C. E. Patton, Phys. Rev. B **77**, 054427 (2008).

[20] I. Barsukov, P. Landeros, R. Meckenstock, J. Lindner, D. Spoddig, Z.-A. Li, B. Krumme, H. Wende, D. L. Mills, and M. Farle, Phys. Rev. B **85**, 014420 (2012).
[21] H. Kurebayashi, T. D. Skinner, K. Khazen, K. Olejník, D. Fang, C. Ciccarelli, R. P. Campion, B. L. Gallagher, L. Fleet, A. Hirohata, and A. J. Ferguson, Appl. Phys. Lett. **102**, 062415 (2013).
[22] M. Körner, K. Lenz, R. A. Gallardo, M. Fritzsche, A. Mücklich, S. Facsko, J. Lindner, P. Landeros, and J. Fassbender, Phys. Rev. B **88**, 054405 (2013).
[23] R. O. Cunha, J. Holanda, L. H. Vilela-Leão, A. Azevedo, R. L. Rodríguez-Suárez, and S. M. Rezende, Appl. Phys. Lett. **106**, 192403 (2015).
[24] R. E. Camley, Phys. Rev. B **89**, 214402 (2014).
[25] V. Castel, N. Vlietstra, B. J. van Wees, and J. Ben Youssef, Phys. Rev. B **90**, 214434 (2014).
[26] A. Y. Dobin and R. H. Victora, Phys. Rev. Lett. **90**, 167203 (2003).
[27] A. D. Boardman and S. A. Nikitov, Phys. Rev. B **38**, 11444 (1988).
[28] H. Schultheiss, K. Vogt, and B. Hillebrands, Phys. Rev. B **86**, 054414 (2012).
[29] V. V. Kruglyak, S. O. Demokritov, and D. Grundler, J. Phys. D **43**, 264001 (2010).
[30] B. Lenk, H. Ulrichs, F. Garbs, and M. Münzenberg, Phys. Rep. **507**, 107 (2011).
[31] A. Hoffmann and S. D. Bader, Phys. Rev. Appl. **4**, 047001 (2015).
[32] Y. Kajiwara, K. Harii, S. Takahashi, J. Ohe, K. Uchida, M. Mizuguchi, H. Umezawa, H. Kawai, K. Ando, K. Takanashi, S. Maekawa, and E. Saitoh, Nature (London) **464**, 262 (2010).
[33] A. V. Chumak, V. I. Vasyuchka, A. A. Serga, and B. Hillebrands, Nat. Phys. **11**, 453 (2015).
[34] OOMMF User's Guide, http://math.nist.gov/oommf/.
[35] H. B. Callen, J. Phys. Chem. Solids **4**, 256 (1958).
[36] R. C. Lecraw, E. G. Spencer, and C. S. Porter, Phys. Rev. **110**, 1311 (1958).
[37] O. L. S. Lieu, G. C. Alexandrakis, and M. A. Huerta, Phys. Rev. B **16**, 476 (1977).
[38] J. Hellsvik, B. Skubic, L. Nordström, and O. Eriksson, Phys. Rev. B **79**, 184426 (2009).
[39] A. Baral, S. Vollmar, and H. C. Schneider, Phys. Rev. B **90**, 014427 (2014).
[40] N. Bloembergen, Phys. Rev. **78**, 572 (1950).
[41] O. Klein, V. Charbois, V. V. Naletov, and C. Fermon, Phys. Rev. B **67**, 220407 (2003).
[42] S. Trudel, O. Gaier, J. Hamrle, and B. Hillebrands, J. Phys. D Appl. Phys. **43**, 193001 (2010).
[43] S. Y. An, P. Krivosik, M. A. Kraemer, H. M. Olson, A. V. Nazarov, and C. E. Patton, J. Appl. Phys. **96**, 1572 (2004).
[44] S. M. Rezende, R. L. Rodríguez-Suárez, and A. Azevedo, Phys. Rev. B **88**, 014404 (2013).
[45] G. de Loubens, V. V. Naletov, and O. Klein, Phys. Rev. B **71**, 180411 (2005).
[46] K. Baberschke, Phys. Stat. Solidi B **245**, 174 (2008).
[47] D. L. Mills and R. Arias, Physica B: Condens. Matter **384**, 147 (2006).
[48] V. E. Demidov, S. Urazhdin, E. R. J. Edwards, M. D. Stiles, R. D. McMichael, and S. O. Demokritov, Phys. Rev. Lett. **107**, 107204 (2011).
[49] V. Kamberský, Can. J. Phys. **48**, 2906 (1970).
[50] E. Abrahams, Phys. Rev. **98**, 387 (1955).
[51] R. C. Fletcher, R. C. Lecraw, and E. G. Spencer, Phys. Rev. **117**, 955 (1960).
[52] W. H. Rippard, M. R. Pufall, S. Kaka, S. E. Russek, and T. J. Silva, Phys. Rev. Lett. **92**, 027201 (2004).
[53] I. N. Krivorotov, N. C. Emley, J. C. Sankey, S. I. Kiselev, D. C. Ralph, and R. A. Buhrman, Science **307**, 228 (2005).
[54] I. N. Krivorotov, D. V. Berkov, N. L. Gorn, N. C. Emley, J. C. Sankey, D. C. Ralph, and R. A. Buhrman, Phys. Rev. B **76**, 024418 (2007).
[55] R. Lehndorff, D. E. Bürgler, S. Gliga, R. Hertel, P. Grünberg, C. M. Schneider, and Z. Celinski, Phys. Rev. B **80**, 054412 (2009).
[56] A. D. Kent and D. C. Worledge, Nat. Nanotechnol. **10**, 187 (2015).
[57] L. Lu, J. Young, M. Z. Wu, C. Mathieu, M. Hadley, P. Krivosik, and N. Mo, Appl. Phys. Lett. **100**, 022403 (2012).
[58] H. Xi, Y. Shi, and K.-Z. Gao, Phys. Rev. B **71**, 144418 (2005).
[59] X. Zhu, J.-G. Zhu, and R. M. White, J. Appl. Phys. **95**, 6630 (2004).
[60] Z. Zeng, G. Finocchio, and H. Jiang, Nanoscale **5**, 2219 (2013).